RESEARCH ARTICLE

Novel conductive polypyrrole/silk fibroin scaffold for neural tissue repair

Ya-Hong Zhao[1, 2, #], Chang-Mei Niu[3, #], Jia-Qi Shi[3], Ying-Yu Wang[4], Yu-Min Yang[1, 2, *], Hong-Bo Wang[1, *]
1 Key Laboratory of Science and Technology of Eco-textiles, Ministry of Education, Jiangnan University, Wuxi, Jiangsu Province, China
2 Key Laboratory of Neuroregeneration, Co-innovation Center of Neuroregeneration, Nantong University, Nantong, Jiangsu Province, China
3 Medical School, Nantong University, Nantong, Jiangsu Province, China
4 Wen Zheng College, Soochow University, Suzhou, Jiangsu Province, China

Funding: *This study was supported by the National Natural Science Foundation of China, No. 81671823, 81701835; a grant from the National Key Research and Development Program of China, No. 2016YFC1101603; a grant from the Natural Science Research Program of Nantong of China, No. MS12016056.*

Graphical Abstract

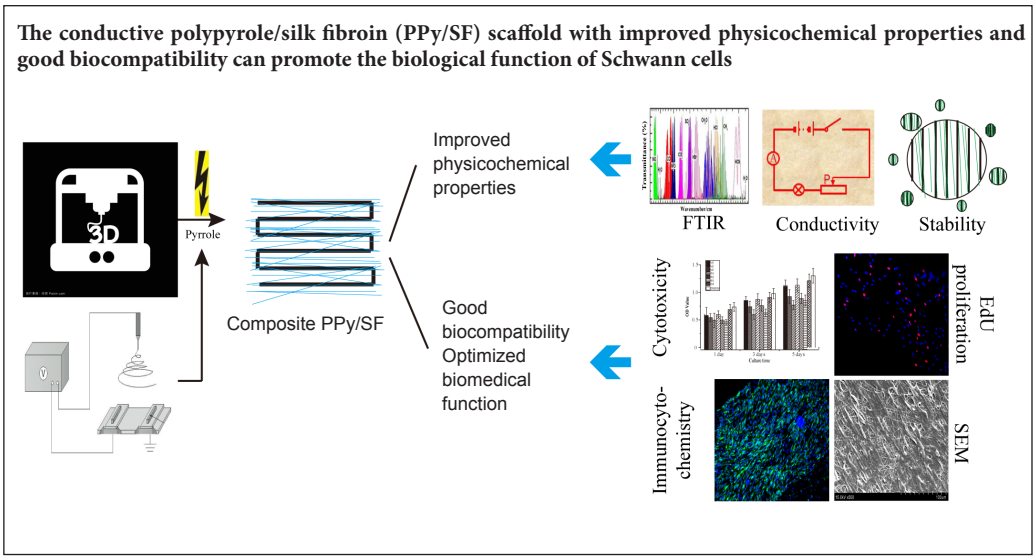

Correspondence to:
Yu-Min Yang, Ph.D. or Hong-Bo Wang, Ph.D., yangym@ntu.edu.cn or wxwanghb@163.com.

#These authors contributed equally to this work.

orcid:
0000-0002-6211-8122 (Ya-Hong Zhao)

doi: *10.4103/1673-5374.235303*

Accepted: *2018-05-28*

Abstract

Three dimensional (3D) bioprinting, which involves depositing bioinks (mixed biomaterials) layer by layer to form computer-aided designs, is an ideal method for fabricating complex 3D biological structures. However, it remains challenging to prepare biomaterials with micro-nanostructures that accurately mimic the nanostructural features of natural tissues. A novel nanotechnological tool, electrospinning, permits the processing and modification of proper nanoscale biomaterials to enhance neural cell adhesion, migration, proliferation, differentiation, and subsequent nerve regeneration. The composite scaffold was prepared by combining 3D bioprinting with subsequent electrochemical deposition of polypyrrole and electrospinning of silk fibroin to form a composite polypyrrole/silk fibroin scaffold. Fourier transform infrared spectroscopy was used to analyze scaffold composition. The surface morphology of the scaffold was observed by light microscopy and scanning electron microscopy. A digital multimeter was used to measure the resistivity of prepared scaffolds. Light microscopy was applied to observe the surface morphology of scaffolds immersed in water or Dulbecco's Modified Eagle's Medium at 37°C for 30 days to assess stability. Results showed characteristic peaks of polypyrrole and silk fibroin in the synthesized conductive polypyrrole/silk fibroin scaffold, as well as the structure of the electrospun nanofiber layer on the surface. The electrical conductivity was 1×10^{-5}–1×10^{-3} S/cm, while stability was 66.67%. A 3-(4,5-dimethyl-2-thiazolyl)-2,5-diphenyl-2-H-tetrazolium bromide assay was employed to measure scaffold cytotoxicity *in vitro*. Fluorescence microscopy was used to observe EdU-labeled Schwann cells to quantify cell proliferation. Immunohistochemistry was utilized to detect S100β immunoreactivity, while scanning electron microscopy was applied to observe the morphology of adherent Schwann cells. Results demonstrated that the polypyrrole/silk fibroin scaffold was not cytotoxic and did not affect Schwann cell proliferation. Moreover, filopodia formed on the scaffold and Schwann cells were regularly arranged. Our findings verified that the composite polypyrrole/silk fibroin scaffold has good biocompatibility and may be a suitable material for neural tissue engineering.

Key Words: *nerve regeneration; composite nanofiber; scaffold; three dimensional bioprinting; electrospinning; silk fibroin; polypyrrole; L929 cells; conductivity; Schwann cells; biocompatibility; nerve repair; neural regeneration*

Introduction

Damage to neural tissues is often caused by trauma or neurological condition, and frequently leads to life-long disability (Adams et al., 2017; Ray et al., 2017). Nerves fail to regenerate and often die following injury or disease, thus motivating the development of a viable, synthetic or biological nerve conduit to overcome limitations of autologous nerve grafts (Grinsell and Keating, 2014; Zhao et al., 2017). However, fabricating feasible nerve grafts with outstanding properties remains a challenge.

The peripheral nervous system involves composite materials with hierarchical structure, each with specific chemical, physical, and topographical properties that as cues for cell behavior; this knowledge helps guide the design of tissue scaffolds (Trappmann et al., 2012; Di Cio and Gautrot, 2016). In addition to these cues, endogenous electric fields have been shown to serve as behavioral cues during nerve reconstruction and neurogenesis (Yao et al., 2011). As a means to achieve this, researchers have investigated electroconductive polymers such as polypyrrole (PPy), polyaniline, and polyphosphazene (Ravichandran et al., 2010; Baniasadi et al., 2015; Gh et al., 2017). PPy has been the most widely studied because of its excellent electrical properties and favorable cell and tissue compatibility. However, its poor solubility and degradation profile demand use of PPy in combination with other biological materials to develop suitable composite materials (Gh et al., 2017; Zhou et al., 2017). As a native protein, silk fibroin (SF) is one of the most interesting polymers being combined with PPy. In addition to excellent biocompatibility, its secondary molecular structure (β-sheets) facilitates combination with PPy (Aznar-Cervantes et al., 2012; Kim et al., 2015).

Topographical regulation of cell alignment is clearly observed in many tissues, generating the need for innovative methods to prepare biomaterials with directional structures (Leigh et al., 2017; Li et al., 2017). Three-dimensional (3D) bioprinting, which involves depositing bioinks (mixed biomaterials) layer by layer to form computer-aided designs, is ideal for fabricating complex 3D biological structures. Indeed, 3D bioprinting offers a broad range of applications for tissue engineering, regenerative medicine, disease modeling, pharmaceutical research, and cancer research (Mandrycky et al., 2016; Ji and Guvendiren, 2017). Although 3D bioprinting technologies have prospects for generating porous materials, it remains challenging to prepare biomaterials with micro-nanostructures that accurately mimic the nanostructural features of natural tissues (Kador et al., 2016; Lee et al., 2017). These characteristics have been matched with a novel nanotechnological tool, electrospinning (Steffens et al., 2017), that permits processing and modification of proper nanoscale biomaterials to enhance neural cell adhesion, migration, proliferation, differentiation, and subsequent nerve regeneration at sites of injury (Wang et al., 2015). Moreover, 3D bioprinting technology can be combined with complex electrospun surfaces to design novel nerve models or therapies.

We hypothesized that integrating electrical, topographical, and chemical cues into a tissue scaffold would offer several advantages over current technologies and promote nerve regeneration. Thus, in this study, a PPy-coated SF (PPy/SF) conductive composite scaffold was fabricated by employing 3D bioprinting and electrospinning. The combination of 3D bioprinting and electrospinning facilitates optimization of the architecture of composite scaffolds to enhance nerve regeneration. The purpose of this study was to evaluate whether a PPy/SF conductive composite scaffold was suitable for neural tissue application.

Materials and Methods

Preparation of PPY/SF scaffolds

Preparation of bioink blend

Bombyx mori silk, purchased from the sericulture provider Xinyuan Co., (Hai'an, Jiangsu, China), was boiled for 30 minutes in 0.5% Na_2CO_3 solution, which was repeated three times. After washing with distilled water several times, degummed silk fibers (20%) were disposed in a ternary solvent system of $CaCl_2/C_2H_5OH/H_2O$ (molar ratio = 1:2:8) at 75 ± 2°C in a thermostatic bath (Xue et al., 2017). To enhance the strength and stability of the scaffold, 10% polyethylene oxide (w/v) was added uniformly to the system at a ratio of 1:10. Solutions were stored in an incubator at room temperature before use.

3D bioprinting scaffolds and PPy coating

A stereolithography-based 3D bioprinter (Regenovo, Hangzhou, China) was employed to print aligned scaffolds. Porous aligned scaffolds with a pre-designed shape were printed under optimized parameters. Specifically, the nozzle insulation temperature and printing chamber temperature were controlled at 4°C and 25°C, respectively, to retain scaffold shape. The nozzle diameter was 0.26 mm. Extrusion speed was adjusted to best fit the nozzle scanning speed. After printing, aligned scaffolds were first treated with 75% ethanol, and then distilled water to remove polyethylene oxide.

Differently aligned PPy/SF was synthesized by coating PPy on an aligned SF scaffold (Lee et al., 2009). To do this, PPy (yellow-brown as received; Aldrich Chemical Company, Milwaukee, WI, USA) was distilled under vacuum to collect colorless liquid, and then the colorless PPy was stored at 4°C in the dark until use. Solutions containing 14 mM pyrrole, 14 mM hydrochloric acid, and 38 mM ferric chloride were prepared separately. The aligned SF scaffold was put into 2 mL of aqueous solution containing 14 mM pyrrole and 14 mM hydrochloric acid in a 60-mm polypropylene dish, followed by ultrasonication for 30 seconds to allow the mesh to be saturated with PPy solution. The scaffold was kept at 4°C for 1 hour. Afterwards, 2 mL of ferric chloride solution (38 mM) was put into the tube and incubated with shaking at 4°C for 24 hours to facilitate polymerization and deposition of PPy on the aligned SF scaffold.

Fabrication of electrospun fiber-3D bioprinted composite scaffolds

Degummed silk fibers were first dissolved in a ternary solvent system of $CaCl_2/C_2H_5OH/H_2O$ (molar ratio = 1:2:8) at 75 ± 2°C in a thermostatic bath, and then dialyzed against

distilled water in a cellulose tube with a 12–14 kDa molecular cutoff for 3 days at room temperature. A portion of the obtained SF aqueous solution was cast in a stainless steel tray, which was dried at room temperature to form SF membranes that were subsequently dissolved in formic acid to acquire 13% (wt/wt) SF spinning solution.

The self-made electrospinning apparatus used in this study consists of three parts: a high-voltage supplier, microinjection pump with a blunt needle serving as an anode, and grounded collection device serving as a cathode. A high electric potential (18–20 kV) was applied to the anode with a needle tip (ID 0.9 mm), into which the droplet of SF spinning solution was loaded. Electrospinning was then continued until a thin layer of SF nanofibers with desired thickness was deposited on the aligned PPy/SF scaffold. After treatment with ethanol for 20 minutes, fabricated PPy/SF composite scaffolds were dried at room temperature.

Characterization of PPY/SF scaffolds

Fourier transform infrared spectroscopy (FTIR)

After samples were cleaned with ethanol and dried, the sample powder was pelleted with potassium bromide and analyzed using a Nexus 870 Fourier transform infrared spectrophotometer (Nicolet Instruments, Madison, WI, USA). All spectra were acquired in the spectral range of 4000–500 cm^{-1}.

Surface morphology analysis

Surface morphology of the PPy/SF membrane was observed using optical microscopy (Leica DMI3000 B, Wetzlar, Germany) and SEM (S-3400 NII; Hitachi, Tokyo, Japan). For SEM observation, briefly, test samples were fixed to an aluminum stage, followed by coating with gold (thickness of ~50 nm). Finally, coated samples were observed by SEM under vacuum (1.33×10^4 Pa) at an acceleration voltage of 20 kV.

Conductivity

To measure electrical conductivity, the resistivity of prepared scaffolds was measured repeatedly by a two-probe method at room temperature using a digital multimeter (Keithley Model 2000, Cleveland, OH, USA). After five measurements, conductivity was estimated using the following formula (Belavi et al., 2012): $\rho = R\pi r^2/t$, where R is the resistance, r is the radius, and t is the thickness of the sample.

Stability

Samples were immersed in water and Dulbecco's Modified Eagle's Medium (DMEM) at 37°C and then shaken (100 r/min) in a sealed container for 30 days. At 0, 3, 5, 10, 20 and 30 days, soaked samples were taken out, and the surface morphology of aligned PPy/SF and composite aligned PPy/SF scaffolds was assessed by optical microscopy.

Biological performance *in vitro*

Cell culture

Mouse fibroblast cells (L929) (Aolu, Shanghai, China) were cultured in a humidified atmosphere of 5% CO_2 in DMEM (Gibco, Carlsbad, CA, USA) at 37°C. The culture medium contained 10% fetal bovine serum (FBS), 100 U/mL penicillin, 100 μg/mL streptomycin, and 4×10^{-3} M L-glutamine.

Primary Schwann cells were prepared from bilateral sciatic nerves collected from 1- to 3-day-old Sprague-Dawley rat pups (provided by the Experimental Animal Center of Nantong University, Jiangsu Province, China), which were enzymatically digested with 0.125% trypsin and 1% collagenase at 37°C for 40 minutes, as previously described (Wang et al., 2016). Next, the mixture was centrifuged at 168 × *g*, resuspended in DMEM with 10% FBS, and the resulting cell suspension was put into petri dishes. After incubation for 24 hours, Schwann cells were purified by adding 10 mM cytosine arabinoside to dishes and incubating for an additional 48 hours to remove fibroblasts. Then, 2 mM forskolin and 2 ng/mL heregulin were added to promote cell proliferation. Thereafter, cells were incubated at 37°C for 7 days in a 5% CO_2 atmosphere before use. After 7-day incubation, primary Schwann cells were digested and cultured on composite PPy/SF samples as follows: composite PPy/SF samples were sterilized in 75% alcohol for 30 minutes and washed twice with sterile deionized water for 2 days to remove unreacted compounds. Subsequently, all sterilized samples were put into a 24-well tissue culture plate and 1 mL of cell suspension was added. The concentration of Schwann cells seeded onto scaffold samples was 1×10^5 cells/mL. All animal protocols were approved by the Animal Care and Use Committee of Nantong University and the Jiangsu Province Animal Care Ethics Committee, and methods were carried out in accordance with approved guidelines.

In vitro cytotoxicity

According to ISO-10993 (Zhang et al., 2013), a 3-(4,5-dimethylthiazol-2-yl)-2,5-diphenyltetrazolium bromide (MTT) assay was performed to determine the *in vitro* cytotoxicity of scaffold extracts. L929 cells were seeded on composite aligned PPy/SF scaffolds in a 24-well plate at a density of 1×10^4 cells per well at 37°C for various time periods; cells cultured in DMEM with 10% FBS were used as a control. After incubation, culture medium from each well was removed and cells were washed three times with phosphate-buffered saline (PBS). Next, 100 μL of MTT solution (5 mg/mL) was added to each well and cells were cultured for an additional 4 hr. The supernatant was discarded and 500 μL of dimethyl sulfoxide was added to each well. OD values of wells were measured on an EIX-800 Microelisa reader at 570 nm (Bio-Tek, Shoreline, WA, USA).

Cell proliferation analyses

A 5-ethynyl-20-deoxyuridine (EdU)-incorporation assay was performed to further investigate Schwann cell proliferation on different composite PPY-SF samples using an EdU labeling/detection kit (Ribobio, Guangzhou, China) according to the manufacturer's instructions. In brief, 50 mM EdU labeling medium was added to cell culture medium and cells were incubated for 12 hours at 37°C in 5% CO_2. Cells were fixed with 4% (w/v) paraformaldehyde for 30 minutes,

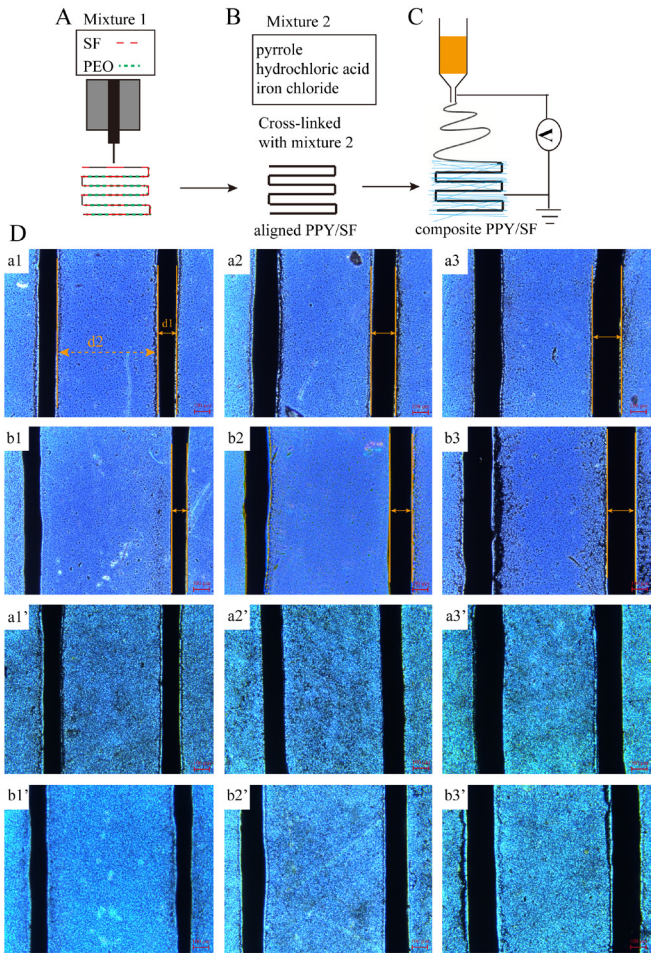

Figure 1 Schematic overview of construct generation.
(A) Bioprinting preparation for SF aligned scaffolds. (B) Polymerization of PPy for SF aligned scaffolds. (C) Coating of electrospun SF nanofibers on aligned PPy/SF scaffolds. (D) Surface morphology of aligned PPy/SF scaffolds with varying diameters and distances (a1–b3): a1-80/500, a2-120/500, a3-180/500, b1-80/700, b2-120/700, and b3-180/700. Surface morphology of aligned PPy/SF scaffolds coupled with electrospun SF nanofiber coating with varying diameters and distances (a1'–b3'): a1'-80/500, a2'-120/500, a3'-180/500, b1'-80/700, b2'-120/700, and b3'-180/700. The number in front of the slash represents the diameter of PPy/SF scaffolds, while the number behind the slash represents the distance between channels of PPy/SF scaffolds. Scale bars: 100 μm. SF: Silk fibroin; PPy: polypyrrole; PEO: polyethylene oxide.

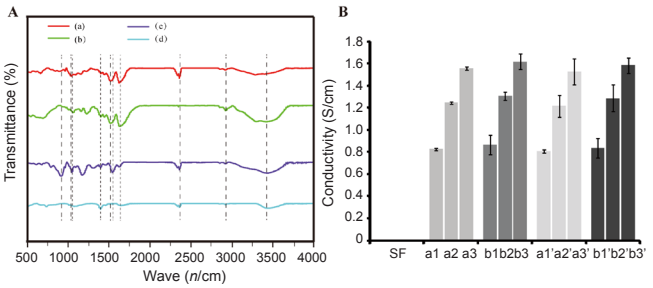

Figure 2 Physicochemical properties of scaffolds.
(A) Fourier transform infrared spectra of composites: (a) PPy; (b) 3D-printed SF treated with ethanol; (c) PPy-coated 3D-printed SF; (d) Py. Dotted lines represent characteristic peaks. (B) Electrical conductivity of different 3D bioprinted aligned SF scaffolds. Aligned PPy/SF scaffolds of varying diameters and distances (a1–b3): a1-80/500, a2-120/500, a3-180/500, b1-80/700, b2-120/700, and b3-180/700. Composite PPy/SF scaffolds with varying diameters and distances (a1'–b3'): a1'-80/500, a2'-120/500, a3'-180/500, b1'-80/700, b2'-120/700, and b3'-180/700. The number in front of the slash represents the diameter of PPy/SF scaffolds, while the number behind the slash represents the distance between channels of PPy/SF scaffolds. Data represent mean ± SEM. An unpaired two-tailed Student's *t*-test was used to evaluate comparisons between two groups. For multiple-group comparisons, one-way analysis of variance with Bonferroni's *post hoc* test was performed to estimate differences among group means. All experiments were carried out in triplicate. SF: Silk fibroin; PPy: polypyrrole; 3D: three-dimensional.

followed by incubation with glycine for 5 minutes. After washing with PBS, cells were reacted with anti-EdU working solution for 30 minutes at room temperature. Afterwards, cells were washed with 0.5% TritonX-100, methanol, and PBS, sequentially, and then stained with 5 mg/mL Hoechst 33342 for 30 minutes at room temperature. Subsequently, cells were observed using laser-scanning confocal microscopy (Leica). Proliferation rates of cells from different samples were evaluated in terms of percentage of EdU-positive cells, as calculated from 10 random fields in three wells.

Immunocytochemistry

After 3 days of culturing Schwann cells in composite PPy/SF samples or complete medium, samples were fixed in 4% paraformaldehyde for 30 minutes at room temperature, washed three times with PBS, and n incubated for 1 hour with blocking buffer containing 3% bovine serum albumin, 10% goat serum, and 0.1% Triton-X 100. Next, samples were reacted with rabbit anti-rat S100β monoclonal antibody (1:200; Abcam) in a humidified chamber overnight at 4°C. After washing three times with PBS, samples were incubated with 488-labeled goat anti-rabbit IgG (1:400; Sigma) in the dark at 4°C for 24 hours. After three washes with PBS, samples were stained with 5 μg/mL Hoechst 33342 (Sigma) at room temperature for 30 minutes, and washed at least three times in PBS. All samples were imaged on a fluorescence microscope (Leica).

SEM

After 3 days of culture, the morphology of adherent Schwann cells cultured in composite PPy/SF samples or complete medium was examined by SEM. First, all samples were dehydrated in sequence with increasing alcohol concentrations (50%, 70%, 80%, 90%, and 100%; $V_{alcohol}/V_{demineralized\ water}$), and then dried at room temperature. Thereafter, samples were coated with 10 nm of gold and images were acquired.

Statistical analysis

Data are presented as mean ± SEM in graphs. Measurements of significant differences between means were performed using SPSS 19.0 software (IBMA Analytics, Armonk, NY, USA). An unpaired two-tailed Student's *t*-test was used to evaluate differences between two groups. For multiple-group comparisons, one-way analysis of variance with Bonferroni's *post hoc* test was performed to estimate differences among group means. A value of $P < 0.05$ was considered statistically significant.

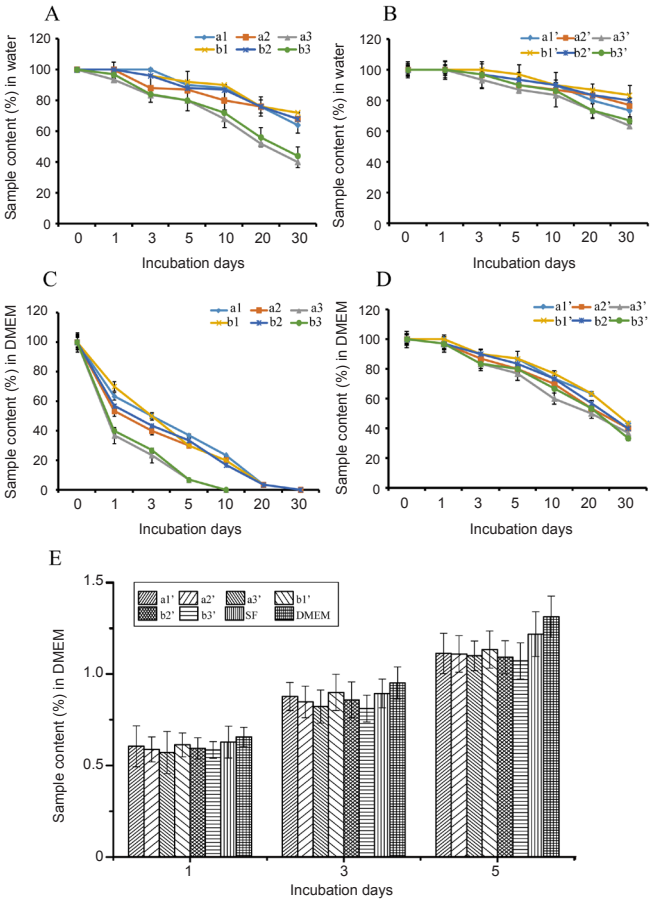

Figure 3 Biological function of scaffolds, as assessed by stability and cytotoxicity.

(A) Percentage of retained aligned PPy/SF samples after incubation in water at 37°C. (B) Equalized percentage of retained composite PPy/SF scaffolds in water at 37°C. (C) Percentage of retained aligned PPy/SF samples at 37°C after immersion in DMEM. (D) Equilibrium percentage of retained composite PPy/SF samples in DMEM at 37°C. Aligned PPy/SF scaffolds with varying diameters and distances (a1–b3): a1-80/500, a2-120/500, a3-180/500, b1-80/700, b2-120/700, and b3-180/700. Composite PPy/SF scaffolds with varying diameters and distances (a1'–b3'): a1'-80/500, a2'-120/500, a3'-180/500, b1'-80/700, b2'-120/700, and b3'-180/700. The number in front of the slash represents the diameter of PPy/SF scaffolds, while the number behind the slash represents the distance between channels of PPy/SF scaffolds. The higher the sample content, the more stability the scaffold exhibited. Percentage of retained scaffolds in different groups was assessed after 1 month. (E) Variation in cell viability of L929 cells, as determined by 3-(4,5-dimethyl-2-thiazolyl)-2,5-diphenyl-2-H-tetrazolium bromide assay, following culture in DMEM or differently aligned PPy/SF or composite aligned PPy/SF scaffold extraction fluids for 1, 3, and 5 days. The viability of L929 cells cultured on different scaffolds indicated no significant difference over time. In addition, the amount of L929 cells increased over time. Data represent mean ± SEM. An unpaired two-tailed Student's *t*-test was used to evaluate comparisons between two groups. For multiple-group comparisons, one-way analysis of variance with Bonferroni's *post hoc* test was performed to estimate differences among group means. All experiments were carried out in triplicate. $*P < 0.05$, *vs.* DMEM group (one-way analysis of variance). SF: Silk fibroin; PPy: polypyrrole; DMEM: Dulbecco's Modified Eagle's Medium; OD: optical density.

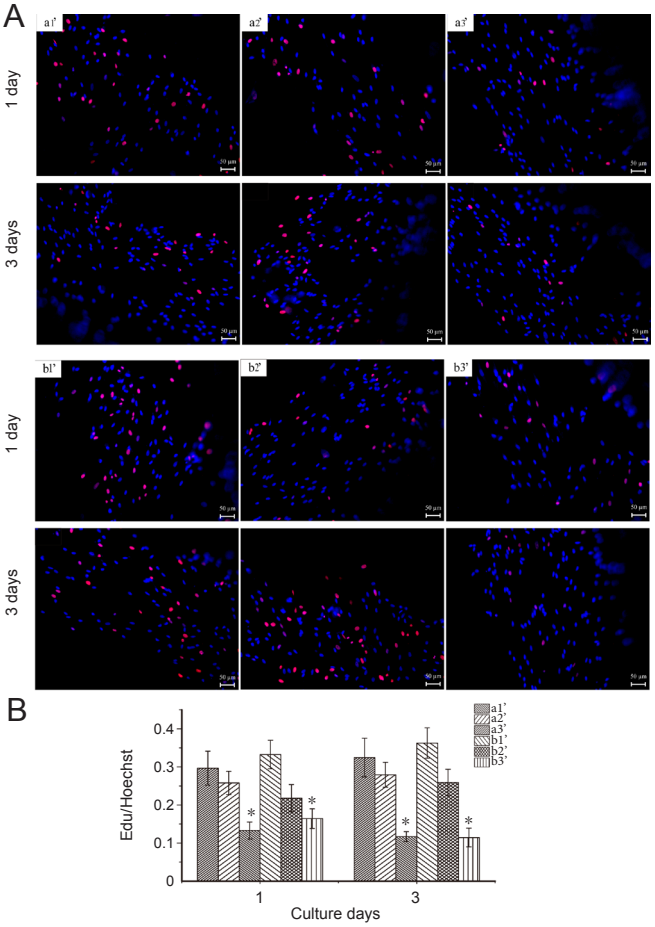

Figure 4 Proliferation of Schwann cells seeded on various PPy/SF composite scaffolds as determined by EdU staining and Hoechst 33342 labeling.

(A) Proliferation of Schwann cells seeded on PPy/SF composite scaffolds with varying diameters and distances: a1'-80/500, a2'-120/500, a3'-180/500, b1'-80/700, b2'-120/700, and b3'-180/700. The number in front of the slash represents the diameter of PPy/SF scaffolds, while the number behind the slash represents the distance between channels of PPy/SF scaffolds after 1 or 3 days in culture, as determined by EdU staining. Merged image of EdU-positive Schwann cells (red) and Hoechst 33342 labeling of cell nuclei (blue). Scale bars: 50 μm. (B) Proliferation of Schwann cells cultured on a3' and b3' was significantly lower than in other groups at all time points. Number of EdU-positive cells on all composite scaffolds increased over time during 3 days of culture. The major trend of proliferation indicated that the proliferation rate decreased as diameter increased. Data represent mean ± SEM. $*P < 0.05$ *vs.* other two diameter scaffolds with the same distance (one-way analysis of variance). All experiments were carried out in triplicate. SF: Silk fibroin; PPy: polypyrrole; EdU: 5-ethynyl-20-deoxyuridine.

Results

Fabrication and characterization of composite scaffolds

Morphology and structure of PPy/SF scaffolds

This study developed a novel and innovative composite fabrication system that combines electrospinning with 3D bioprinting, thus eliminating one of the main limitations of 3D bioprinting alone. **Figure 1** shows the manufacturing process.

Designed nozzles smoothly deposit the optimized bioink in the form of aligned scaffolds with different transverse scales, which is achieved by regulating the size of the needles. As tiny differences in bioprinting parameters have large influences on scaffold properties, we investigated the effect of different sizes on electrical conductivity and biological function of cells. In total, six PPy/SF scaffolds were characterized as aligned: a1-80/500, a2-120/500, a3-180/500, b1-80/700, b2-120/700, and b3-180/700. Each has a different diameter (d1) and distance (d2); the number in front of the slash represents the diameter of the PPy/SF scaffold, while the number behind the slash represents the distance between channels of the PPy/SF scaffold. Electrically conductive aligned scaffolds were generated by applying the polymerizing PPy process to preformed cross-linked aligned SF scaffolds (**Figure 1D**) under optimized conditions. PPy/SF aligned scaffolds maintained the primary aligned structure, which was similar to non-coated template scaffolds. The resulting scaffolds with an interpenetrating PPy and SF network, characterized as a1'–b3', appeared to be macroscopically homogenous and had black features indicating PPy. By combining electrospinning with bioprinting, we are able to generate tissue constructs containing a layer of electrospun SF nanofibers (**Figure 1D**).

FTIR spectra characterization

To characterize structural changes in SF, Py, PPy, and PPy/SF scaffolds, FTIR was performed (**Figure 2A**). Peaks in the region of 1527 cm^{-1} and 1627 cm^{-1} were attributed to the secondary NH bending of amide-II and C=O stretching of amide-I, respectively, which were ascribed to the presence of β-sheets in SF (**Figure 2A-b**). The main characteristic IR absorption spectra of PPy (**Figure 2A-a**) revealed that C-H stretching vibrations of PPy appeared at 2923 cm^{-1} and peaked at 1457 and 1547 cm^{-1}, which was attributed to the C-N and C-C stretching vibration of pyrrole rings, respectively, as well as a band at 1633 cm^{-1} corresponding to C=C stretching.

After deposition of PPy on aligned SF scaffolds, some absorption bands associated with vibrational modes corresponding to the conjugated polymers appeared in the spectra of resulting materials. In the case of PPy/SF, bands appeared near 1020 cm^{-1} and 800 cm^{-1}, which were ascribed to the C-N in-plane deformation mode and C-H wagging of PPy, respectively. The presence of both SF and PPy conformed to their homologous infrared absorption characteristic peaks of SF and PPY in the spectrum of PPy/SF. The band at 1630 cm^{-1} is a characteristic peak of SF. The two bands at 1544 cm^{-1} and 1040 cm^{-1} are characteristic PPy peaks. All three peaks are present in the PPy/SF spectrum, verifying that the composite PPy/SF was successfully synthesized.

Conductivity

The electrical properties of different materials were characterized via measurement of the conductivity of resulting scaffolds, as described in the Materials and Methods section. Pristine 3D bioprinted aligned SF scaffolds did not display any appreciable conductivity (sensitivity of the instrument was 1×10^{-11} S/cm). In contrast, aligned PPy/SF scaffolds and composite PPy/SF scaffolds showed conductivities in the region of 1×10^{-5}–1×10^{-3} S/cm (**Figure 2B**). The results indicates that deposited PPy polymers formed a coating on the fibers that constituted an effectively homogenous and continuous path to promote conductivity in the resulting scaffolds. The bulk conductivity of pure aligned PPy/SF was $1.82 \pm 0.21 \times 10^{-5}$ S/cm to $1.13 \pm 0.19 \times 10^{-3}$ S/cm, increasing with aligned diameter. The results indicated that the electrical conductivity increased as the size of aligned diameter (d1) increased, but was not related to distance (d2). Therefore, aligned scaffolds with bigger diameter exhibit a larger electrical conductivity compared with smaller scaffolds. In addition, incorporation of electrospun SF nanofibers negatively affected the electrical properties of PPy/SF aligned scaffolds. Electrospun-coating in relaxed states was observed from $1.65 \pm 0.12 \times 10^{-5}$ S/cm to $1.09 \pm 0.22 \times 10^{-3}$ S/cm (**Figure 2B**). Collectively, these results suggest that deposited PPy polymer is useful for forming electrically conductive domains on the surface. Moreover, a thin layer of SF nanofibers coated on the aligned PPy/SF hardly affected the conductivity of resulting scaffolds.

Stability of composite PPy/SF scaffolds

The stability of scaffolds was evaluated in by incubating aligned PPy/SF and composite PPy/SF scaffolds in water and DMEM over the course of 30 days. PPy mixed with small anions was brittle according to previous reports, thus preventing its wide application for long-term performance (Green et al., 2008). Our 4-week stability assay indicated very little debris or delamination of PPy shells in water, but the aligned PPy/SF scaffold, especially samples with a large size (d1) peeled from the substrate when incubation time was prolonged. It was observed that the stability for aligned PPy/SF in water was maintained at 33.33% (**Figure 3A**), while composite PPy/SF scaffolds maintained 66.67% (**Figure 3B**) during the 4-week stability test, which may partly arise from the stabilization effect of the outer-enclosure formed by electrospun SF nanofibers.

In contrast to the results described above, significant fragmentation and/or delamination was observed in DMEM during the 4-week stability test. This was especially notable in samples with a large diameter size (a3, a3', b3, and b3'), which showed increased delamination of PPy shells, distortion, falling, or even collapse of some stripes; indeed, a3 and b3 collapsed at 10 days. Whereas, for the composite sample (**Figure 3D**), parallel stripe-like structures were still clearly observable and maintained during immersion over time, indicating better stability than the aligned sample (**Figure 3C**), as demonstrated by a3' and b3' maintaining 33.33% during the 4-week stability test. These results revealed that graphical construction of PPy/SF aligned micropatterning with a large size could be broken down to a certain degree by DMEM immersion, while PPy/SF aligned micropatterning with a small size was better retained than samples with large size. Furthermore, the stability of composite PPy/SF scaffolds in DMEM was superior to most aligned PPy/SF scaffolds, as

shown in **Figure 3**. This suggests that PPy/SF scaffolds had different stability in water and DMEM, indicating that PPy/SF scaffolds had diverse stability performance in different solutions, while electrospun-coated scaffolds maintain their topography.

Biological performance of composite scaffolds

In vitro cytotoxicity evaluation

The mouse fibroblast L929 cell line is routinely used to evaluate cytotoxicity according to ISO-10993. The *in vitro* cell toxicity of scaffolds was tested using an MTT assay of L929 cells to quantify numbers of living cells. **Figure 3E** shows MTT conversion of L929 cells cultured on scaffolds with varying diameters (PPy contents) at 1, 3 and 5 days. The results indicated a slight reduction of cells on scaffolds compared with control samples (SF) during culture. However, as the number of days increased, number cells on samples gradually increased. According to the decrease of cell activity at day 1, the viability of L929 cells seeded on different samples followed the trend: a1' > a2' > a3', and b1' > b2' > b3'. As cells continued to proliferate, a1' and b1' cells were significantly increased compared with other groups up to day 5. Cell viability was observed to decrease as the diameter of the composite PPy/SF scaffold (d1) increased; although, it was still almost non-toxic (a3', b3'), as cells maintained 97.18% of the relative growth rate compared with DMEM control. The results confirmed that all scaffolds have good biocompatibility and were not toxic to L929 cells (**Figure 3E**). This suggests that the combination of electrospinning and bioprinting did not affect cell viability.

Schwann cell growth on coated fibers

EdU incorporation was carried out to determine the effect of different scaffolds on Schwann cell proliferation. Schwann cells were used to evaluate the biocompatibility of prepared composite scaffolds with different d1 size after seeding Schwann cells on samples for 1 and 3 days. The cell proliferation rate was determined by counting the number of EdU-positive cells from day 1 to day 3. A two-fold increase in the cell proliferation rate was observed in a1' and b1' compared with a3' and b3' (**Figure 4**). In addition, the number of cells on all scaffolds increased over time during the 3 days of culture. The general trend showed that as diameter increased, the propagating rate declined. The maximal number of proliferated Schwann cells in the scaffolds was 29.66% and 32.45% for 1 and 3 days in a1', and 33.22% and 36.27% for b1'. This behavior was attributed to the increased amount of PPy, in good agreement with decreased MTT results shown in **Figure 3E**. This result was consistent with the study by Shi et al. (2008), which indicated that materials with lower amounts of conductive polymers are the best candidates for biomaterial applications.

S100β/Hoechst staining was performed to observe the morphology and spreading of cells on scaffolds. Fluorescence images of Schwann cells stained for S100β (**Figure 5**) indicated cells formed processus pseudopodia on all scaffolds. Pure electrospun SF nanofiber scaffolds were suitable for cell adherence and growth. Compared with control-SF nanofibers, all composite scaffolds revealed lower cell attachment and poorer cell state. Hence, the conjugated PPy coating was found to inhibit cell adhesion, especially in the case of large-diameter samples. This may result from the highly hydrophobic nature of PPy resulting in unsatisfactory cell adherence properties. Considering the main problems associated with using pure PPy, PPy has been blended with other materials to achieve cell attachment (Ateh et al., 2006). These results clearly indicate that PPy coupled with electrospun SF nanofibers is a potential scaffold for nerve tissue engineering.

SEM

SEM images showing typical distribution of Schwann cells after culture on different composite scaffolds of varying sizes for 3 days are shown in **Figure 6**. Cells displayed good distribution with elongated podia. The cells seem to have grown throughout the scaffolds, marking their migration through the nanofiber surface, either on top of the PPy-containing printed construct or in the space between prints. After 3 days of culture, Schwann cells exhibited the good adhesion and spreading, and most cells displayed a spindle-like morphology with long filopodia. Filopodia of different cells connected to each other and formed a network, indicating strong cell-cell interactions. The cellular layer is clearly observable on the surface, indicating the compatibility of composite PPy/SF scaffolds. As exhibited in **Figure 6**, although SF nanofibers on the surface of scaffolds were randomly distributed without orientation, Schwann cells displayed a spindle-shaped morphology and aligned arrangement. This may be attributed to the fact that polymerization leads to the organization of a film with some level of aligned organization (Gh et al., 2017).

Discussion

In this study, 3D bioprinting and electrospinning were combined to fabricate conductive composite PPy/SF scaffolds with aligned conduction and nanofiber structures. Physicochemical assessments showed improved performance compared with SF or PPy alone. Furthermore, an assessment of biological function using neuroglial cells also displayed an improvement, indicating that conductive composite PPy/SF scaffolds are potentially useful as a neural tissue material.

Our results demonstrated that polymerization resulted in the precipitation of PPy formations. It is proposed that these are then simply adsorbed at the aligned 3D SF scaffolds, as confirmed by FTIR of aligned 3D PPy/SF scaffolds. Fibroin is relatively hydrophobic with a high content of aromatic amino acids, which may favor the adsorption of conjugated polymers *via* hydrophobic interactions or π-stacking. Moreover, natural peptide linkages (-CO-NH-) in SF may also contribute to enhancing polymerization *via* hydrogen-bonding and electrostatic interactions. Moreover, the electrospinning coating process preserved the morphology, structure, and most physical properties of aligned 3D PPy/SF scaffolds, and resulted in nanofibers forming on the surface.

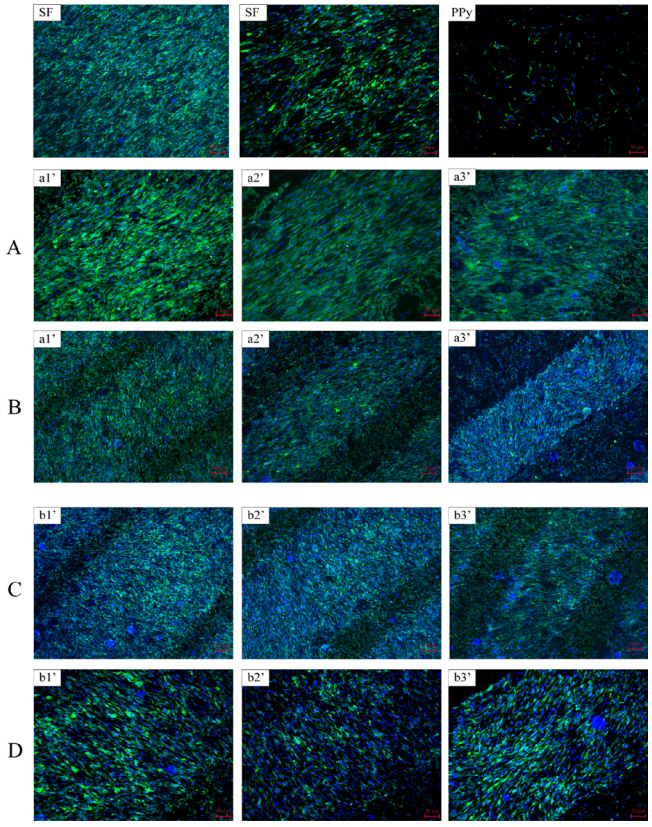

Figure 5 Immunofluorescence staining of Schwann cells with anti S100β and Hoechst after 3 days of culture.
Immunofluorescence staining of Schwann cells with anti S100β and Hoechst after 3 days of culture on various PPy/SF composite scaffolds with varying diameters and distances: a1'-80/500, a2'-120/500, a3'-180/500, b1'-80/700, b2'-120/700, and b3'-180/700. The number in front of the slash represents the diameter of PPy/SF scaffolds, while the number behind the slash represents the distance between channels of PPy/SF scaffolds. Merged image of immunofluorescence staining for S100β (green) and Hoechst 33342 labeling of cell nuclei (blue). (A, D) Magnified image of samples in B, C. Scale bars: 100 μm for B, C; 50 μm for A, D. All composite scaffolds showed good cell attachment and proliferation, and improved problems associated with pure PPy. SF: Silk fibroin; PPy: polypyrrole.

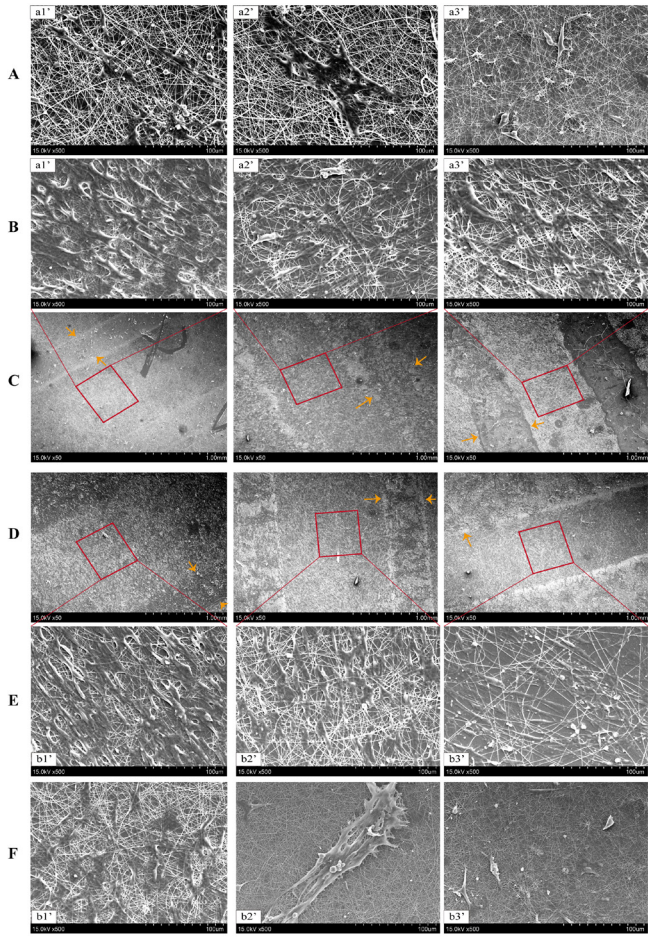

Figure 6 Scanning electron microscopy micrographs of Schwann cells cultured on various PPy/SF composite scaffolds at 3 days in culture.
(A, B) Magnification of the space between prints (square frame) and on top of PPy structures (arrows) in C; (E, F) magnification of square frames and arrows in D. Scale bars: 1 mm for C, D; 100 μm for A, B, E, F. After 3 days of culture, Schwann cells exhibited good adhesion and spreading, showing strong cell-cell interactions. The cellular layer is clearly observable on the surface, indicating compatibility of composite PPy/SF scaffolds. Orange arrows indicate the border of aligned scaffolds. SF: Silk fibroin; PPy: polypyrrole.

Preservation of the architecture of resulting composite PPy/SF scaffolds was confirmed by morphologic observation. The results indicated that deposited PPy polymers formed a coating on scaffolds that constituted an relatively homogenous and continuous path to promote conductivity in resulting scaffolds. Conductivity experiments demonstrated that increasing the amount of PPy proportional to 3D bioprinting diameter greatly increased the electrical properties of the scaffold, while electrospinning coating had little effect. This observation indicated the pivotal role played by the amount of PPy doped onto SF scaffolds in determining their final electrical conductivity. However, stability tests indicated that aligned 3D PPy/SF scaffolds are brittle, while composite PPy/SF scaffolds are stable; thus, composite PPy/SF scaffolds were used for biological assessments.

To explore the potential of composite PPy/SF scaffolds in the biomedical field, for example, as implantable electrodes in nerves, their cytocompatibility and ability to sustain cell adhesion were characterized. To examine the compatibility of composite PPy/SF scaffolds, *in vitro* cytotoxicity tests of scaffold extracts against L929 cells were conducted according to ISO-10993. L929 cells are routinely used for *in vitro* cytotoxicity studies because they are easy to prepare and culture (Cintra et al., 2017). Composite PPy/SF scaffolds displayed no obvious cytotoxicity and were a good substrate for the growth of L929 cells. In addition, biomedical functional evaluation of composite scaffolds was performed using Schwann cells, which are glial cells found in the peripheral nervous system that play a vital role in the regeneration and repair of injured nerves. The results showed that Schwann cells mainly adhered to the surface of scaffolds, whereby they maintained their normal configuration (plump, spindle-shaped and glossy), connected to each other, and proliferated well on all composite PPy/SF scaffolds. These results

demonstrate that the conductive composite PPy/SF scaffolds showed good compatibility with L929 cells and may enhance Schwann cell adhesion, differentiation, and proliferation.

It is also demonstrated that topographical effects may be further enhanced by electrical and chemical cues to promote nerve regeneration (Jamal and de Guzman, 2017). These studies show that in designing the next generation of biomaterials, stimulation signals should be considered to better mimic the biological microenvironment. Considering the beneficial effect of electrical stimulation on nerve regeneration (Baniasadi et al., 2015; Kabiri et al., 2015), ongoing studies are focused on investigating the effects of conductive composite scaffolds coupled with electrical stimulation on the functional response of Schwann cells.

Our results are consistent with previous results (Liao et al., 2014; Bhattacharjee et al., 2016) demonstrating the function of electrospun silk scaffolds and bioactivity of PPy-coated materials in favor of cell attachment, growth, and spreading. In conclusion, while peripheral nerve injury remains a common clinical problem, tissue-engineered nerve grafts have shown potential to facilitate regeneration and functional recovery (Tian et al., 2015). Although many efforts have been made (Madduri et al., 2010; Jenkins et al., 2015; Zhao et al., 2017), it remains a challenge to fabricate feasible nerve grafts with outstanding properties. Thus, the ability to utilize topological structures, electrical stimulation, and improved biomaterials is advantageous. Among these complex cues, an important aspect of synthetic nerve grafts is their ability to conduct electricity, as well as their nanoscale features (Mobini et al., 2017; Poggetti et al., 2017). Conductive nanofibrous scaffolds allow for nerve cell migration and promote nerve regeneration (Jin and Li, 2014). Composite conductive scaffolds used in the current study were manufactured using a novel approach involving a combination of PPy deposition on 3D-bioprinted SF scaffolds and electrospun SF fibers. Composite PPy/SF scaffolds integrated topographical and electrical cues within the scaffold, which is advantageous for providing an alternative to nerve autografts. However, as all our conclusions rely on biological assessment *in vitro*, the effect of composite conductive scaffolds on functional nerve recovery still needs to be investigated *in vivo*. In addition, the exact effects of composite conductive scaffolds are not fully understood and, thus, precise mechanisms require further investigation.

Author contributions: *YHZ designed the study, performed experiments, and wrote the paper. CMN and JQS performed experiments. YMY and HBW designed the study and revised the paper. YYW collected and analyzed the data. All authors approved the final version of the paper.*
Conflicts of interest: *There are no conflicts of interest to declare.*
Financial support: *This study was supported by the National Natural Science Foundation of China, No. 81671823, 81701835; a grant from the National Key Research and Development Program of China, No. 2016YFC1101603; a grant from the Natural Science Research Program of Nantong of China, No. MS12016056. None of the funding bodies play any role in the study.*
Institutional review board statement: *All experimental procedures were approved by the Animal Care and Use Committee of Nantong University and the Jiangsu Province Animal Care Ethics Committee. The experimental procedure followed the National Institutes of Health Guide for the Care and Use of Laboratory Animals (NIH Publications No. 8023, revised 1985).*
Copyright license agreement: *The Copyright License Agreement has been signed by all authors before publication.*
Data sharing statement: *Datasets analyzed during the current study are available from the corresponding author on reasonable request.*
Plagiarism check: *Checked twice by iThenticate.*
Peer review: *Externally peer reviewed.*

Open peer review report:
Reviewer: *Tufan Mert, University of Cukurova, Turkey.*
Comments to authors: *In the paper, the authors have mainly tested the combined polypyrole/silk fibroin conductive composite scaffold on in vitro for its ability to influence the behavior and functions of Schwann cells. Main suggestion of this manuscript is that combined polypyrole/silk fibroin matrix would be an effective material in cell culture and tissue engineering, where electrical conduction properties are required. Efforts of authors are valuable from a scientific viewpoint. This is an interesting study, and the study procedures and examinations are well performed and provide reliable results. I have no complaint regarding the presented data.*

References

Adams AM, VanDusen KW, Kostrominova TY, Mertens JP, Larkin LM (2017) Scaffoldless tissue-engineered nerve conduit promotes peripheral nerve regeneration and functional recovery after tibial nerve injury in rats. Neural Regen Res 12:1529-1537.

Ateh DD, Navsaria HA, Vadgama P (2006) Polypyrrole-based conducting polymers and interactions with biological tissues. J R Soc Interface 3:741-752.

Aznar-Cervantes S, Roca MI, Martinez JG, Meseguer-Olmo L, Cenis JL, Moraleda JM, Otero TF (2012) Fabrication of conductive electrospun silk fibroin scaffolds by coating with polypyrrole for biomedical applications. Bioelectrochemistry 85:36-43.

Baniasadi H, Ramazani SAA, Mashayekhan S (2015) Fabrication and characterization of conductive chitosan/gelatin-based scaffolds for nerve tissue engineering. Int J Biol Macromol 74:360-366.

Belavi PB, Chavan GN, Naik LR, Somashekar R, Kotnala RK (2012) Structural, electrical and magnetic properties of cadmium substituted nickel–copper ferrites. Mater Chem Phys 132:138-144.

Bhattacharjee P, Kundu B, Naskar D, Kim HW, Bhattacharya D, Maiti TK, Kundu SC (2016) Potential of inherent RGD containing silk fibroin-poly (capital JE, Ukrainian-caprolactone) nanofibrous matrix for bone tissue engineering. Cell Tissue Res 363:525-540.

Cintra LTA, Benetti F, de Azevedo Queiroz IO, Ferreira LL, Massunari L, Bueno CRE, de Oliveira SHP, Gomes-Filho JE (2017) Evaluation of the cytotoxicity and biocompatibility of new resin epoxy-based endodontic sealer containing calcium hydroxide. J Endod 43:2088-2092.

Di Cio S, Gautrot JE (2016) Cell sensing of physical properties at the nanoscale: Mechanisms and control of cell adhesion and phenotype. Acta Biomater 30:26-48.

Gh D, Kong D, Gautrot J, Vootla SK (2017) Fabrication and characterization of conductive conjugated polymer-coated antheraea mylitta silk fibroin fibers for biomedical applications. Macromol Biosci 17.

Green RA, Lovell NH, Wallace GG, Poole-Warren LA (2008) Conducting polymers for neural interfaces: challenges in developing an effective long-term implant. Biomaterials 29:3393-3399.

Grinsell D, Keating CP (2014) Peripheral nerve reconstruction after injury: a review of clinical and experimental therapies. Biomed Res Int 2014:698256.

Jamal D, de Guzman RC (2017) Silicone substrate with collagen and carbon nanotubes exposed to pulsed current for MSC osteodifferentiation. Int J Biomater 2017:3684812.

Jenkins PM, Laughter MR, Lee DJ, Lee YM, Freed CR, Park D (2015) A nerve guidance conduit with topographical and biochemical cues: potential application using human neural stem cells. Nanoscale Res Lett 10:972.

Ji S, Guvendiren M (2017) Recent advances in bioink design for 3D bioprinting of tissues and organs. Front Bioeng Biotechnol 5:23.

Jin G, Li K (2014) The electrically conductive scaffold as the skeleton of stem cell niche in regenerative medicine. Mater Sci Eng C Mater Biol Appl 45:671-681.

Kabiri M, Oraee-Yazdani S, Shafiee A, Hanaee-Ahvaz H, Dodel M, Vaseei M, Soleimani M (2015) Neuroregenerative effects of olfactory ensheathing cells transplanted in a multi-layered conductive nanofibrous conduit in peripheral nerve repair in rats. J Biomed Sci 22:35.

Kador KE, Grogan SP, Dorthe EW, Venugopalan P, Malek MF, Goldberg JL, D'Lima D D (2016) Control of retinal ganglion cell positioning and neurite growth: combining 3D printing with radial electrospun scaffolds. Tissue Eng Part A 22:286-294.

Kim SY, Naskar D, Kundu SC, Bishop DP, Doble PA, Boddy AV, Chan HK, Wall IB, Chrzanowski W (2015) Formulation of biologically-inspired silk-based drug carriers for pulmonary delivery targeted for lung cancer. Sci Rep 5:11878.

Lee JY, Bashur CA, Goldstein AS, Schmidt CE (2009) Polypyrrole-coated electrospun PLGA nanofibers for neural tissue applications. Biomaterials 30:4325-4335.

Lee SJ, Nowicki M, Harris B, Zhang LG (2017) Fabrication of a highly aligned neural scaffold via a table top stereolithography 3D printing and electrospinning. Tissue Eng Part A 23:491-502.

Leigh BL, Truong K, Bartholomew R, Ramirez M, Hansen MR, Guymon CA (2017) Tuning surface and topographical features to investigate competitive guidance of spiral ganglion neurons. ACS Appl Mater Interfaces 9:31488-31496.

Li S, Kuddannaya S, Chuah YJ, Bao J, Zhang Y, Wang D (2017) Combined effects of multi-scale topographical cues on stable cell sheet formation and differentiation of mesenchymal stem cells. Biomater Sci 5:2056-2067.

Liao J, Zhu Y, Yin Z, Tan G, Ning C, Mao C (2014) Tuning nano-architectures and improving bioactivity of conducting polypyrrole coating on bone implants by incorporating bone-borne small molecules. J Mater Chem B 2014:7872-7876.

Madduri S, Papaloizos M, Gander B (2010) Trophically and topographically functionalized silk fibroin nerve conduits for guided peripheral nerve regeneration. Biomaterials 31:2323-2334.

Mandrycky C, Wang Z, Kim K, Kim DH (2016) 3D bioprinting for engineering complex tissues. Biotechnol Adv 34:422-434.

Mobini S, Leppik L, Thottakkattumana Parameswaran V, Barker JH (2017) In vitro effect of direct current electrical stimulation on rat mesenchymal stem cells. PeerJ 5:e2821.

Poggetti A, Battistini P, Parchi PD, Novelli M, Raffa S, Cecchini M, Nucci AM, Lisanti M (2017) How to direct the neuronal growth process in peripheral nerve regeneration: future strategies for nanosurfaces scaffold and magnetic nanoparticles. Surg Technol Int 30:458-461.

Ravichandran R, Sundarrajan S, Venugopal JR, Mukherjee S, Ramakrishna S (2010) Applications of conducting polymers and their issues in biomedical engineering. J R Soc Interface 7 Suppl 5:S559-579.

Ray WZ, Mahan MA, Guo D, Guo D, Kliot M (2017) An update on addressing important peripheral nerve problems: challenges and potential solutions. Acta Neurochir (Wien) doi: 10.1007/s00701-017-3203-3.

Shi G, Rouabhia M, Meng S, Zhang Z (2008) Electrical stimulation enhances viability of human cutaneous fibroblasts on conductive biodegradable substrates. J Biomed Mater Res A 84:1026-1037.

Steffens D, Mathor MB, Soster P, Vergani G, Luco DP, Pranke P (2017) Treatment of a burn animal model with functionalized tridimensional electrospun biomaterials. J Biomater Appl 32:663-676.

Tian L, Prabhakaran MP, Ramakrishna S (2015) Strategies for regeneration of components of nervous system: scaffolds, cells and biomolecules. Regen Biomater 2:31-45.

Trappmann B, Gautrot JE, Connelly JT, Strange DG, Li Y, Oyen ML, Cohen Stuart MA, Boehm H, Li B, Vogel V, Spatz JP, Watt FM, Huck WT (2012) Extracellular-matrix tethering regulates stem-cell fate. Nat Mater 11:642-649.

Wang Y, Zhao Y, Sun C, Hu W, Zhao J, Li G, Zhang L, Liu M, Liu Y, Ding F, Yang Y, Gu X (2016) Chitosan degradation products promote nerve regeneration by stimulating Schwann cell proliferation via miR-27a/FOXO1 axis. Mol Neurobiol 53:28-39.

Wang YL, Gu XM, Kong Y, Feng QL, Yang YM (2015) Electrospun and woven silk fibroin/poly(lactic-co-glycolic acid) nerve guidance conduits for repairing peripheral nerve injury. Neural Regen Res 10:1635-1642.

Xue C, Zhu H, Tan D, Ren H, Gu X, Zhao Y, Zhang P, Sun Z, Yang Y, Gu J, Gu Y, Gu X (2017) Electrospun silk fibroin-based neural scaffold for bridging a long sciatic nerve gap in dogs. J Tissue Eng Regen Med doi: 10.1002/term.2449.

Yao L, Pandit A, Yao S, McCaig CD (2011) Electric field-guided neuron migration: a novel approach in neurogenesis. Tissue Eng Part B Rev 17:143-153.

Zhang L, Dou S, Li Y, Yuan Y, Ji Y, Wang Y, Yang Y (2013) Degradation and compatibility behaviors of poly(glycolic acid) grafted chitosan. Mater Sci Eng C Mater Biol Appl 33:2626-2631.

Zhao Y, Wang Y, Gong J, Yang L, Niu C, Ni X, Wang Y, Peng S, Gu X, Sun C, Yang Y (2017) Chitosan degradation products facilitate peripheral nerve regeneration by improving macrophage-constructed microenvironments. Biomaterials 134:64-77.

Zhou X, Yang A, Huang Z, Yin G, Pu X, Jin J (2017) Enhancement of neurite adhesion, alignment and elongation on conductive polypyrrole-poly(lactide acid) fibers with cell-derived extracellular matrix. Colloids Surf B Biointerfaces 149:217-225.

(*Copyedited by Deusen AV, Yajima W, Yu J, Li CH, Qiu Y, Song LP, Zhao M*)